Central European Journal of Energetic Materials
ISSN 1733-7178; e-ISSN 2353-1843

Cent. Eur. J. Energ. Mater. 2024, *21*(2): 113-137; DOI 10.22211/cejem/186614
Article is available in PDF-format, in colour, at:
https://ipo.lukasiewicz.gov.pl/wydawnictwa/cejem-woluminy/vol-21-nr-2/

Research paper

Study on the Spatial Distribution of Natural Fragments Based on Fractal Model of Fragment Mass Distribution

Xian Xu Huo[1)], **Wei Bing Li**[1),*)], **Jian Jun Zhu**[2)]
[1)] *Nanjing University of Science and Technology, China*
[2)] *China Helicopter Research and Development Institute, China*
* *E-mail:* njustlwb@163.com

Abstract: In order to solve the problem of using fragment quantity spatial distribution to describe fragment spatial distribution, this paper proposes a fragment mass probability density model to describe fragment spatial distribution. Applying the idea of stress gradient and velocity gradient grade in the process of explosion, the calculation equation of fragment direction angle at different axial positions of warhead is established. Based on the fractal model of natural fragment mass distribution in the form of Weibull function, a two-dimensional joint probability density model of fragment scattering space angle and fragment mass is established, and the model is verified by tests. The research results show that when the space angle is between 90° and 100°, the theoretical calculation error of fragment mass distribution is 4.3%, and the theoretical calculation error of fragment quantity distribution is 19.4%, compared with the test results. This shows that the fragment mass spatial distribution is more suitable for characterizing the fragment spatial distribution law than the fragment quantity spatial distribution. When considering the characteristics of non-uniform fragment mass formed in different regions of warhead, the prediction accuracy of the fragment mass spatial distribution model established in this paper is 18.2% higher than that of previous models, which can more accurately reflect the fragment spatial distribution law.

Keywords: fragment spatial distribution, Shapiro equation, fractal model of fragment mass distribution, anti-personnel warhead, numerical simulation

1 Introduction

Cylindrical metal shell is a common structure of weapon warhead. The cylindrical metal shell will form a large number of fragments after the internal explosive detonates. The velocity distribution, size distribution, mass distribution and spatial distribution of fragments are of great value to the damage effectiveness evaluation of weapon and protective structure design. For a long time, scholars have made rich and effective achievements in the research of fragment size distribution, velocity distribution and mass distribution [1-7]. For fragment mass distribution, scholars have always used Mott equation or Payman equation to describe it. However, with the application of new materials and new explosives, a large number of tests have found that Mott equation and other theories have large errors in describing the fragment mass distribution [8-10]. Zhu [11] established a mathematical model of fragment mass distribution in the form of dual parameter Weibull distribution on the basis of the volume fractal dimension of particles proposed by Yang [12], and subsequently studied the effects of warhead geometry, explosive properties, shell material properties and other factors on shell fragmentation, solving the problem that Mott equation did not consider shell properties and explosive properties.

The spatial scattering characteristics, spatial distribution of fragment quantity and spatial distribution of fragment mass are of great significance for describing the spatial distribution of fragments [13]. Shapiro equation is widely used in engineering because it can simply and accurately calculate the scattering angle of fragments, but there is a large error in the calculation results of Shapiro equation when describing the scattering angle of warhead end fragments [14]. In the past, scholars [14, 15] described the fragment spatial distribution law through the fragment spatial quantity density distribution. They assume that the average mass of fragments formed in any interval is the same, which is obviously inconsistent with the actual situation [16]. For the fragment mass spatial distribution, Karpp [17] recovered fragments from various regions of the spherical target when studying the fragment spatial distribution of the 105 mm high explosive (HE) warhead. The study found that the fragment mass spatial distribution can be expressed by a function that is approximate to the normal distribution function, but the author did not give a fragment mass spatial distribution model. Therefore, it is urgent to study the mathematical model to accurately describe the fragment spatial distribution.

Aiming at the problems in the description of fragment spatial distribution and based on previous research results. In this paper, firstly, the calculation equation of fragment direction angle formed at different axial positions of

warhead is established based on the idea of stress gradient and velocity gradient grade in the process of explosion, and the scattering of fragments in space after warhead explosion is obtained. Secondly, based on the fractal model of natural fragment mass distribution in the form of Weibull function, a two-dimensional joint probability density model of fragment scattering space angle and fragment mass is established to describe the fragment mass distribution in the fragment scattering space. The model is verified by fragment recovery test based on the principle of spherical target test, and the difference of fragment quantity and fragment mass in different space areas is explained.

2 Study on Spatial Scattering Characteristics of Fragments

2.1 Shapiro equation correction

Shapiro assumes that the warhead is composed of many rings arranged continuously, and the centers of the rings are on the axis of symmetry of the warhead shell. Detonation wave starts from the initiation point and spreads outward in the form of spherical wave front. As shown in Figure 1 below, the normal of the warhead shell forms an included angle φ_1 with the symmetry axis of the warhead shell, and the detonation wave normal forms an included angle φ_2 with the symmetry axis of the warhead shell. The fragment velocity direction angle is γ, the deflection angle θ of fragment velocity vector deviating from the warhead shell normal, Shapiro equation is [18]:

$$\tan\theta = \frac{v_0}{4D_e}\cos\left(\frac{\pi}{2} - \phi_1 + \phi_2\right) \tag{1}$$

where θ is the deflection angle between the fragment velocity vector and the normal of the warhead, φ_1 is the angle formed between the normal of the warhead and the symmetry axis of the warhead, φ_2 is the angle formed between the normal of the detonation wave and the symmetry axis of the warhead, v_0 is the fragment velocity, D_e is the detonation velocity.

According to the geometric relationship, the fragment velocity direction angle is:

$$\gamma = \frac{\pi}{2} - \phi_1 + \tan^{-1}\left[\frac{v_0}{4D_e}\cos\left(\frac{\pi}{2} - \phi_1 + \phi_2\right)\right] = \frac{\pi}{2} - \phi_1 + \theta \tag{2}$$

where γ is the fragment velocity direction angle (the deflection angle between the velocity vector and y axis).

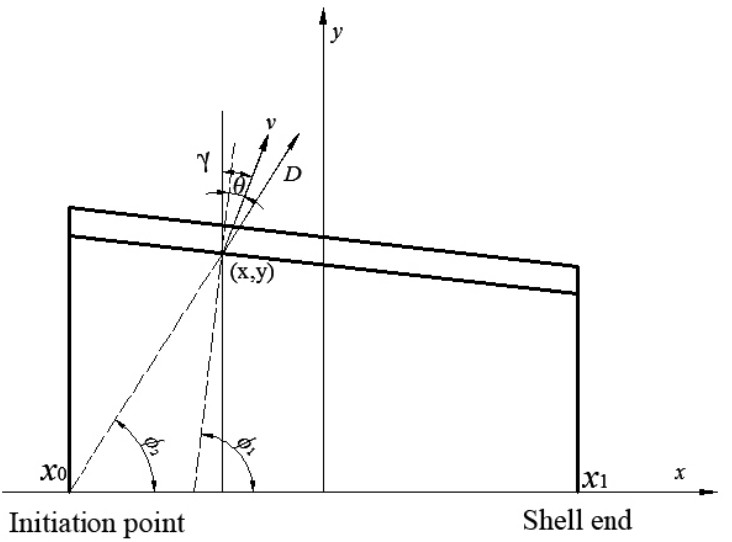

Figure 1. Schematic diagram of fragment scattering angle

Due to the difference in the impact of detonation wave and rarefaction wave on different axial positions of the shell, the fragment velocity and fragment scattering direction at different axial positions of the shell are different, so Shapiro equation cannot truly reflect the fragment scattering. The fragment velocity changes from positive to negative, and the divergence angle changes from negative to positive. From the motion equation of fluid theory, it can be seen that the change of velocity reflects the change of stress in the shell, so the fragment scattering angle can be corrected by using the term of velocity gradient.

For cylindrical shells under single point initiation at the center of the end face, according to Shapiro equation, the fragment velocity direction angle is:

$$\tan\gamma = \tan\theta = \frac{v_0}{4D_e}\cos\phi_2 \tag{3}$$

According to the theory put forward by Huang [19], the change rule of fragment velocity along the shell axis under different conditions can be described by Equation 3a:

$$F(x) = [1 - A_* \exp(-B_* \cdot x)] \cdot [1 - C_* \exp(-D_* \cdot (1 - x))] \tag{3a}$$

similar to the exponential form. Therefore, based on the exponential form equation, taking into account the influence of shell length diameter ratio and relative wall thickness, this paper establishes the fragment velocity distribution equation along the shell axis:

$$\begin{cases} v_{0x} = F(x)\cdot\sqrt{2E_{G\sigma}}\sqrt{\dfrac{C/M}{1+0.5C/M}} \\ F(x) = \left[1 - A_* \exp\left(-B_* \cdot \dfrac{L}{d}\left(\dfrac{\delta}{d}\right)^{k_1} \cdot x\right)\right] \\ \qquad \cdot\left[1 - C_* \exp\left(-D_* \cdot \dfrac{L}{d}\left(\dfrac{\delta}{d}\right)^{k_1} \cdot (1-x)\right)\right] \end{cases} \tag{4}$$

where $x(0 \le x \le 1)$ is the axial relative position of the shell. A_*, B_*, C_*, D_* and k_1 are all undetermined constants. $E_{G\sigma} = \dfrac{D^2}{2(\gamma^2-1)} \cdot \left[1 - 2\left(\dfrac{2\sigma_s}{\sqrt{3}P_0}\right)^{\frac{\gamma-1}{\gamma}} \cdot \left(\dfrac{\gamma}{\gamma+1}\right)^{\gamma}\right]$ is the Gurney energy related to the yield stress of the shell material [21], L/d is the length-diameter ratio of warhead, δ/d is the relative wall thickness of warhead, $F(x)$ is the fragment velocity correction term, M is the mass of the shell and C is the mass of the explosive.

$x_0/(x_1 - x_0) \le x \le x_1/(x_1 - x_0)$, $L = x_1 - x_0$ needs to be defined in combination with Figure 1, so the fragment velocity equation is:

$$\begin{cases} v_{0x} = F(x)\cdot\sqrt{2E_{G\sigma}}\sqrt{\dfrac{C/M}{1+0.5C/M}} \\ F(x) = \left[1 - A_* \exp\left(-B_*\cdot\dfrac{L}{d}\left(\dfrac{\delta}{d}\right)^{k_1}\cdot\left(x - \dfrac{x_0}{x_1 - x_0}\right)\right.\right. \\ \qquad \cdot\left[1 - C_* \exp\left(-D_*\cdot\dfrac{L}{d}\left(\dfrac{\delta}{d}\right)^{k_1}\cdot\left(\dfrac{x_1}{x_1 - x_0} - x\right)\right.\right. \end{cases} \quad 5$$

According to the motion equation of the fluid, the deflection angle θ of the velocity vector of the fragment from the shell normal is corrected by using the velocity gradient term, and from the relationship between the deflection angle θ and the velocity direction angle γ, we can get:

$$\tan\gamma = \tan\theta = \frac{v_0}{4D_e}\left[F(x)\cdot\cos\phi_2 - k_2\frac{dF(x)}{dx}\right] \quad 6$$

where $k_2(k_2 > 0)$ is the correction factor.

2.2 Calculation of fragment movement direction angle

In order to obtain the spatial scattering distribution of fragments along the axis of the warhead, taking the general structure of the kill warhead as an example, it is divided into three parts: arc part, cylinder part and ship tail, as shown in Figure 2. The coordinate of a certain point on the warhead is (x, y), and the deflection angle between the velocity vector and axis of the point is γ. Taking the warhead centroid as the center of the circle, make a sphere with radius R, and the target is on the sphere. The coordinate of a fragment hitting the target is (l, h) and φ is the motion direction angle of the fragment at the hit point. Taking the inner wall curve of warhead as the research object, the geometric relationship in Figure 2 is as follows:

$$\begin{cases} l - x = (h - y)\tan\gamma \\ l^2 + h^2 = R^2 \\ \tan\varphi = l/h \end{cases} \quad (7)$$

where (l, h) is the coordinate of the target hit by the fragment, (x, y) is the

coordinate of a certain point on the warhead, φ is the motion direction angle of the fragment at the hit point, R is the radius of the fragment field.

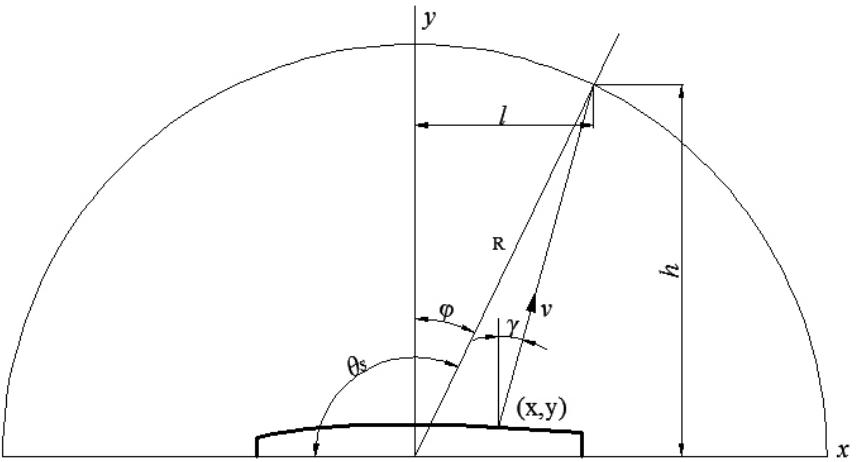

Figure 2. Fragment scattering diagram of warhead

Making:

$$\begin{cases} l_1 = l - x \\ h_1 = h - y \end{cases} \tag{8}$$

According to Equations 7 and 8:

$$\begin{cases} l_1 = h_1 \tan\gamma \\ (l_1 + x)^2 + (h_1 + y)^2 = R^2 \end{cases} \tag{9}$$

According to Equation 9:

$$(h_1 \tan\gamma + x)^2 + (h_1 + y)^2 = R^2 \tag{10}$$

Further operation on Equation 10:

$$h_1^2 \tan^2\gamma + 2h_1 x \tan\gamma + x^2 + h_1^2 + 2h_1 y + y^2 = R^2 \tag{11}$$

Finally:

$$h_1 = \sqrt{\left(y + x\tan\gamma\right)^2 \cos^2\gamma + R^2 - x^2 - y^2} \cdot \cos\gamma - \left(y + x\tan\gamma\right)\cos^2\gamma \tag{12}$$

Combined Equation 9 and 12:

$$l_1 = \sqrt{\left(y + x\tan\gamma\right)^2 \cos^2\gamma + R^2 - x^2 - y^2}\,\sin\gamma - \left(y + x\tan\gamma\right)\cos\gamma\sin\gamma \tag{13}$$

According to Equation 7:

$$\tan\varphi = \frac{l_1 + x}{h_1 + y} \tag{14}$$

Assume that the curve function of the inner wall of the warhead is:

$$y = y(x) \tag{15}$$

According to Equation 6:

$$\gamma = \gamma\left(x\right) = \arctan\left(\frac{v_0}{4D_e}\left[F(x)\cdot\cos\phi_2 - k_2\frac{dF(x)}{dx}\right]\right) \tag{16}$$

According to Equation 14, the fragment movement direction angle can be expressed as:

$$\varphi = F\left(x, y(x), \gamma(x)\right) \tag{17}$$

where x and y are basic parameters of warhead. The following focuses on solving $y(x)$.

2.3 Numerical solution of velocity direction angle

It is difficult to measure the scattering angle of fragments in tests. The finite element simulation software can simulate the whole process of warhead fragment formation, and can obtain the fragment movement direction and

fragment velocity field distribution at different parts of the warhead axis by setting measurement points. Therefore, in order to determine the undetermined coefficients, AUTODYN finite element software is used to simulate the fragment formation process of the kill warhead to obtain fragment velocity data and fragment movement direction data at different axial positions of the warhead. Finally, these data are used to fit the corresponding equation.

A three-dimensional finite element model was established as shown in Figure 3, and simplified into two parts: the explosive and the cylindrical shell. Due to the symmetry of the cylindrical shell, only a 1/4 model was established. The shell material is 50SiMnVB steel, and the main mechanical parameters are from reference [20]. The four schemes of 8701, Comp-B, TNT, and CL-20-based mixed explosives were used for the charge, and the property parameters are from reference [24, 25]. The detonation method is single-point detonation at the centre of one end of the casing. The Lagrange algorithm was used for the casing, the ALE algorithm was used for the charge, and the grid size was 1 mm. The expansion process of the detonation products after the explosive's detonation is described by the JWL state equation [25]. Johnson-Cook model is widely used to describe the mechanical response of metallic materials subjected to large strains, high strain rates, and high temperatures [26]. The state equation adopts linear form, and the Stochastic random failure model is used to simulate the formation of natural fragments.

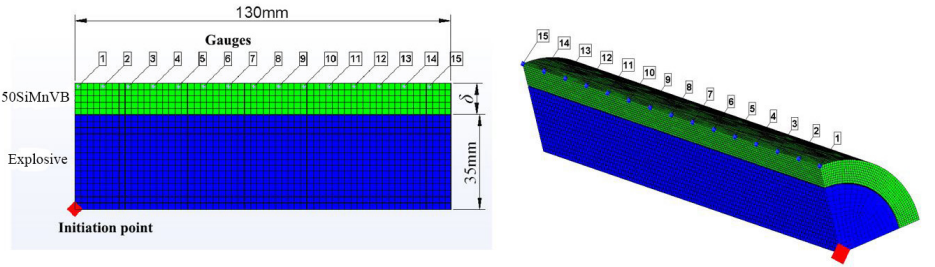

Figure 3. Numerical simulation model and test point location

Table 1. Main parameters of shell material model

Material	Tempering temperature [°C]	*A* [MPa]	*B* [MPa]
50SiMnVB	550	1047	262
	n	*m*	*C*
	0.028	0.63	0.018

Table 2. C-J parameters of detonation products of explosives

Explosive	ρ_0 [g·cm^{-3}]	D [km·s^{-1}]	p_{CJ} [GPa]	e [kJ·cm^{-3}]
CL-20	1.94	9.06	39.3	10.02
Comp B	1.72	7.79	28.3	8.31
TNT	1.63	6.93	21.0	6.00
JH-2	1.70	8.43	30.4	10.20

Table 3. Parameters of JWL equation of state for explosive detonation products

Explosive	A [GPa]	B [GPa]	R_1	R_2	ω
CL-20	875.0	30.00	4.73	1.39	0.26
Comp B	524.3	7.67	4.20	1.10	0.34
TNT	373.8	3.75	4.15	0.90	0.35
JH-2	852.4	18.02	4.60	1.30	0.38

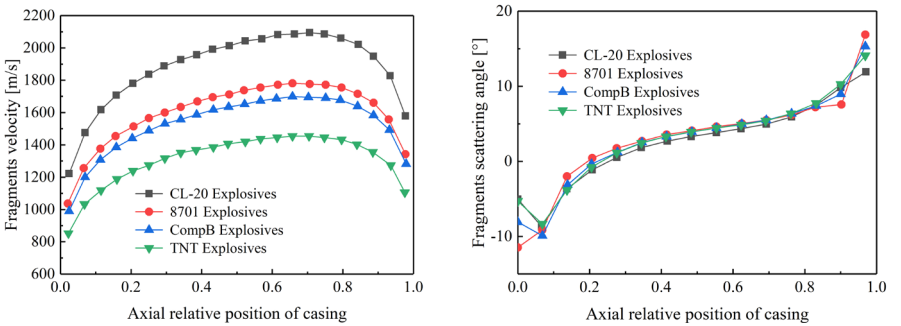

(a) (b)

Figure 4. Scattering characteristics of fragments velocity (a) and scattering angle (b)

Display the data obtained by simulation in Figure 4. As shown in Figure 4(a), the velocity of fragments formed by 50SiMnVB shells under the loading of four kinds of explosives has a similar trend along the axial direction, that is, the initial velocity of fragments formed is the smallest near the initiation point of explosives, and the maximum initial velocity of fragments appears at about 63% of the cylinder length from the initiation point. The scattering angle of the fragments formed by the shell under the four kinds of explosives is basically the same, and the variation trend along the axial direction of the shell is also the same. This shows that the properties of explosives have no effect on the scattering angle of fragments. The previous theoretical analysis shows that the warhead geometry has a great influence on the fragment scattering angle.

Fitting Equations 5 and 6 through simulation data. The velocity distribution of the fragment along the axial direction of the shell after considering the aspect ratio of the shell and the relative wall thickness of the shell is:

$$\begin{cases} v_{0x} = F(x)\cdot\sqrt{2E_{G\sigma}}\sqrt{\dfrac{C/M}{1+0.5C/M}} \\ F(x) = \left[1-0.424\exp\left(-0.686\cdot\dfrac{L}{d}\left(\dfrac{\delta}{d}\right)^{-0.5}\cdot\left(x-\dfrac{x_0}{x_1-x_0}\right)\right)\right] \\ \qquad\cdot\left[1-0.315\exp\left(-1.666\cdot\dfrac{L}{d}\left(\dfrac{\delta}{d}\right)^{-0.5}\cdot\left(\dfrac{x_1}{x_1-x_0}-x\right)\right)\right] \end{cases} \tag{18}$$

The scattering angle of the fragments formed by the cylindrical warhead is:

$$\tan\gamma = \tan\theta = \frac{v_0}{4D_e}\left[F(x)\cdot\cos\phi_2 - 5.405\frac{dF(x)}{dx}\right] \tag{19}$$

According to the geometric relationship in Figure 1:

$$\cos\phi_2 = \frac{x-x_0}{\sqrt{(x-x_0)^2+y^2}} = \frac{x-x_0}{\sqrt{(x-x_0)^2+r^2}} \tag{20}$$

where r is the radius of the shell at x, $r = y(x)$.

Combined Equations 19 and 20:

$$\tan\gamma = \tan\theta = \frac{v_0}{4D_e}\left[F(x)\cdot\frac{x-x_0}{\sqrt{(x-x_0)^2+r^2}} - 5.405\cdot\frac{dF(x)}{dx}\right] \tag{21}$$

Firstly, the basic parameters of warhead are used to calculate the fragmentation velocity direction angle $\gamma(x) = (\vec{v}\,\hat{}\,y)$ under any warhead structure by Equations 18 and 21. Then, by combining Equations 12 and 13 and $\begin{cases} l_1 = l - x \\ h_1 = h - y \end{cases}$, the coordinate ($l$, h) of the fragment hit point can be calculated. Finally, the motion direction angle φ of the fragment at $R = \sqrt{l^2 - h^2}$ was calculated by equation:

$$\tan\varphi = l/h \tag{21a}$$

3 Study on Spatial Distribution of Fragment Mass

3.1 Theoretical model

Assume that within the interval [θ_S, $\theta_S + d\theta_S$], the fragment mass is dM. The total mass of the fragments formed by the warhead is M_0, then the mass probability density of the fragments to the space is:

$$\rho_M(\theta_s) = \frac{dM}{M_0 d\theta_s} \tag{22}$$

where is the total mass of fragments formed by the warhead.

According to Equation 22, the spatial mass density of the fragment between the scattering region is (θ_1, θ_{i+1}) and the fragment mass (m_i, m_{i+1}) is:

$$\rho_M\left((\theta_i \sim \theta_{i+1}),(m_i \sim m_{i+1})\right) \tag{23}$$

or:

$$\rho_M(\theta_s, \mathrm{m}) = \frac{dM}{M_0 \cdot d\theta_s \cdot dm} \tag{24}$$

In view of the spatial distribution results of fragment mass, scholars [17] recovered fragments in each area of the spherical target when studying 105 mm HE warhead. It is found that the spatial distribution of fragment mass can also be expressed by a normal distribution, as shown in Figure 5.

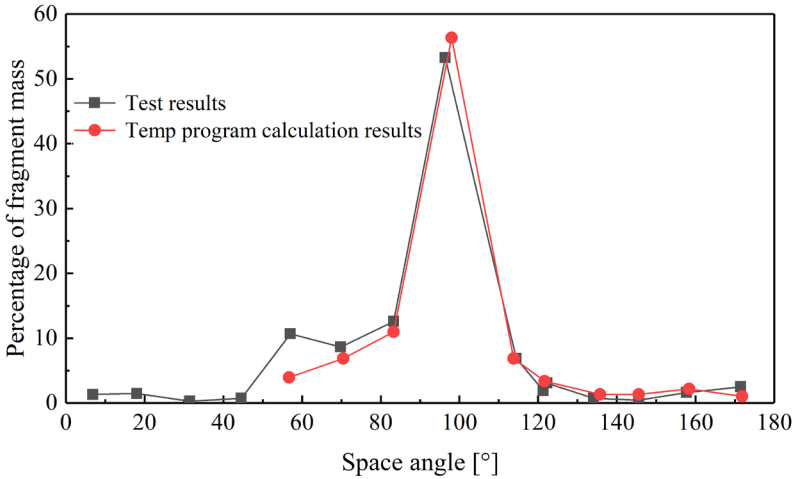

Figure 5. Spatial distribution results of fragment relative mass [17]

Therefore, this paper introduces the normal distribution form into the spatial distribution function of fragment mass. In combination with the fragment mass distribution model based on volume fractal dimension proposed by Zhu [11] and the normal distribution property of space angle, Equation 24 is:

$$\rho_M(\theta_s, m) = \frac{dM}{M_0 \cdot d\theta_s \cdot dm} = \frac{1}{\sqrt{2\pi}\sigma} e^{-\frac{(\theta_s-\theta_0)^2}{2\sigma^2}} \cdot \frac{dM_-}{dm} \tag{25}$$

or:

$$\rho_M(\theta_s, m) = \frac{1}{\sqrt{2\pi}\sigma} e^{-\frac{(\theta_s-\theta_0)^2}{2\sigma^2}} \ln 2 \left(m/\bar{m}_M\right)^{\lambda-1} \cdot \left(\lambda/\bar{m}_M\right) \exp\left[-\ln 2 \left(m/\bar{m}_M\right)^{\lambda}\right] \tag{26}$$

where $\lambda = \frac{2D_3 - 4}{3 - D_3}$, D_3 is the volume fractal dimension of fragment, $\bar{m}_M$ is average mass of fragments.

Equation 26 reflects that the fragment mass meets the normal distribution to the spatial angle. The closer the space angle θ_s is to the mathematical expectation of θ_0, the greater the cumulative value of fragment mass. With different mass of

fragments, the spatial distribution is also different. The closer the spatial angle θ_s is to θ_0, the greater the mass of fragments is. Mean square deviation σ can be considered as a function of fragment mass m: $\sigma = \sigma(m)$. Large mass fragments are more concentrated, while small mass fragments are more dispersed. Combining with the theory proposed by predecessors [22], it can be believed that $\sigma(m)$ decreases with the increase of fragment mass m.

According to the fragment mass distribution function adopted in this paper, it can be assumed that:

$$\sigma=\sigma_0\left[k_t+\exp\left[-\ln 2(m/\bar{m}_M)^{\frac{2D_3-4}{3-D_3}}\right]\right] \tag{27}$$

where σ_0 and k_t are test constants, generally $k_t = 0.5$. For small mass fragments (m tends to 0), $\sigma = 1.5\sigma_0$, and for large mass fragments, $\sigma = 0.5\sigma_0$.

The spatial distribution law of fragment mass can be obtained by solving the expected value of space angle , the mean mass of fragment [23], the volume fractal dimension D_3 [11] and the initial mean square error σ_0.

3.2 Solving the expected value and mean square error of space angle

The warhead is divided into several small units along the axial direction. According to Figure 1, in the centroid coordinate system, the initial position (x_i, y_i) of each fragment and the total mass M_{0i} of the fragment are known. According to the corresponding equation in Section 2, the motion direction angle of the fragment at the radius R of the scattering region can be calculated as follows: $\varphi(x_i) = F(x_i)$ and $\theta_s = \frac{\pi}{2} + \varphi$. According to Equation 24:

$$\rho_M(\varphi,m)=\frac{dM}{M_0\cdot d\varphi\cdot dm} \tag{28}$$

According to the definition of expected value and variance, we can obtain:

$$E(\varphi)=\iint\rho_M(\varphi,m)\cdot\varphi\cdot d\varphi\cdot dm=\iint\frac{\varphi}{M_0}dM \tag{29}$$

$$D(\varphi)=\iint\rho_M(\varphi,m)\cdot(\varphi-\varphi_0)^2\cdot d\varphi\cdot dm=\iint\frac{(\varphi-\varphi_0)^2}{M_0}dM \tag{30}$$

Therefore:

$$\varphi_0 = \iint \frac{\varphi}{M_0} dM \tag{31}$$

$$\sigma_0^2 = \iint \frac{(\varphi - \varphi_0)^2}{M_0} dM \tag{32}$$

In consideration of engineering practicability and known total fragment mass M_{0i} and distribution of fragment motion angle in any area along the warhead axis, Equations 31 and 32 are approximated:

$$\varphi_0 = \frac{\sum_{i=1}^{n} \varphi_i M_{0i}}{M_0} \tag{33}$$

$$\sigma_0^2 = \frac{\sum_{i=1}^{n} (\varphi_i - \varphi_0)^2 M_{0i}}{M_0} \tag{34}$$

According to $\theta_0 = \frac{\pi}{2} + \varphi_0$, the spatial distribution index θ_0 and σ_0 of fragment mass can be obtained. The mass and quantity of fragments in any interval $[\theta_i, \theta_{i+1}; m_i, m_{i+1}]$ can be solved by $\rho_M(\theta_S, m)$ integral:

$$\Delta M = M_0 \int_{\theta_i}^{\theta_{i+1}} \int_{m_i}^{m_{i+1}} \rho_M(\theta_s, m) dm \cdot d\theta_s \tag{35}$$

$$\Delta N = M_0 \int_{\theta_i}^{\theta_{i+1}} \int_{m_i}^{m_{i+1}} \frac{\rho_M(\theta_s, m)}{m} dm \cdot d\theta_s \tag{36}$$

4 Test Verification of the Spatial Distribution Model of Fragment Mass

4.1 Test design

In this paper, the accuracy of the spatial distribution model of fragment mass is verified by the test data of fragment recovery based on the spherical target principle. As shown in Figure 6, the test arrangement followed the principle of spherical target test, but the target plates were replaced by boxes, and boxes were filled with wood chips as the decelerating medium. The open end of the box was covered with thin wooden boards, and boxes were arranged at a distance of 1 mm from the explosion center. A total of 18 boxes were arranged, and the angle of fragment recovery was 15°. The warhead faced the first box. The warhead is made of 45# steel in the test. The explosive is JH-14 with a density of 1.69 g·cm^{-3} and the detonation velocity is 8.3 km/s. The Gurney velocity of the fragment is 2.68 km/s. After three tests, fragments were screened from each box and all test data were averaged.

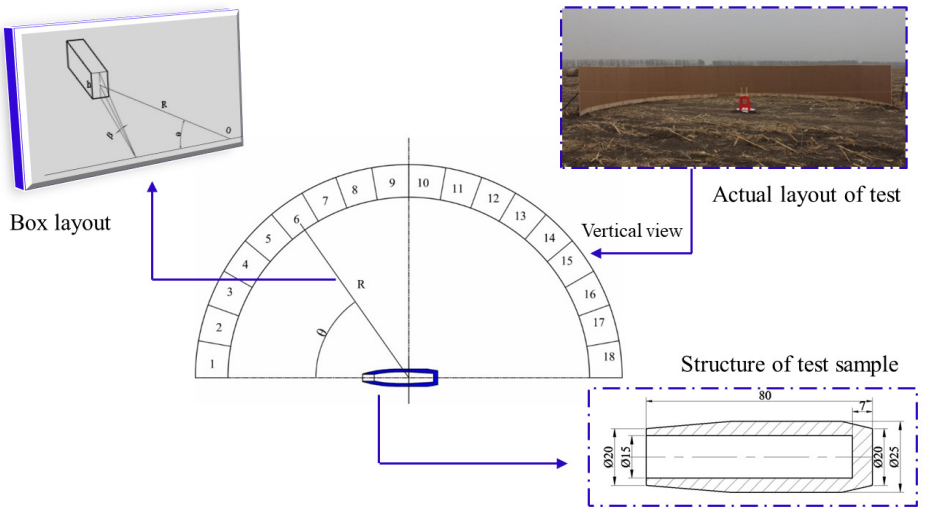

Figure 6. Schematic diagram of the test

The recycling box with a height of h is used to recover the fragments at the center $R = 1$ away from the warhead. Suppose the polar Angle of the center of the box mouth is $\bar{\theta}_i = \dfrac{\theta_i + \theta_{i+1}}{2}$, then the ratio of the box mouth area to the area of the whole ball belt is:

$$\frac{\beta}{2\pi} = \frac{1}{\pi}\arctan\frac{h}{2R\sin\overline{\theta}_i} \tag{37}$$

where β is the angle between the upper and lower boundaries of the recycling box and the axis of the warhead, h is the height of the recycling box. R is the distance between the warhead and the recycling box.

Mass and quantity of fragments in any interval $[\theta_i, \theta_{i+1}; m_i, m_{i+1}]$:

$$\Delta M = M_{Box}\frac{\pi}{\arctan\dfrac{h}{2R\sin\overline{\theta}_i}} \tag{38}$$

$$\Delta N = N_{Box}\frac{\pi}{\arctan\dfrac{h}{2R\sin\overline{\theta}_i}} \tag{39}$$

where M_{Box} and N_{Box} are respectively the mass and quantity of fragments recovered from the i-th box.

4.2 Theoretical calculation of spatial distribution of fragment mass

The warhead is divided into 16 sections along the axial direction, each 5 mm long, and the last two sections are 3 and 7 mm (projectile bottom). According to Equations 18 and 21, the fragment velocity and fragment velocity direction angle at different coaxial positions of the warhead can be calculated. The theoretical results of fragment scattering characteristics are shown in Figure 7. It can be seen from Figure 7 that the shell wall thickness has a great influence on the fragmentation velocity distribution along the axial direction of the warhead. Due to the impact of the geometric structure of the warhead, the velocity direction angle of the fragments at both ends will be inclined to 90°. Therefore, these results are not reflected in Figure 7. With the center of mass of warhead as the starting point, the motion direction angle of the fragment when the fragment scattering space radius is 1 m can be obtained by Equation 17, and the results are shown in Figure 8.

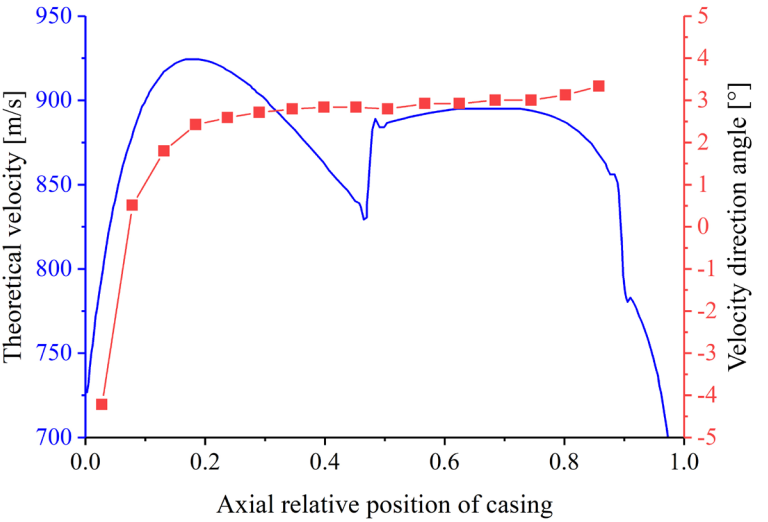

Figure 7. Theoretical results of scattering characteristics of fragments

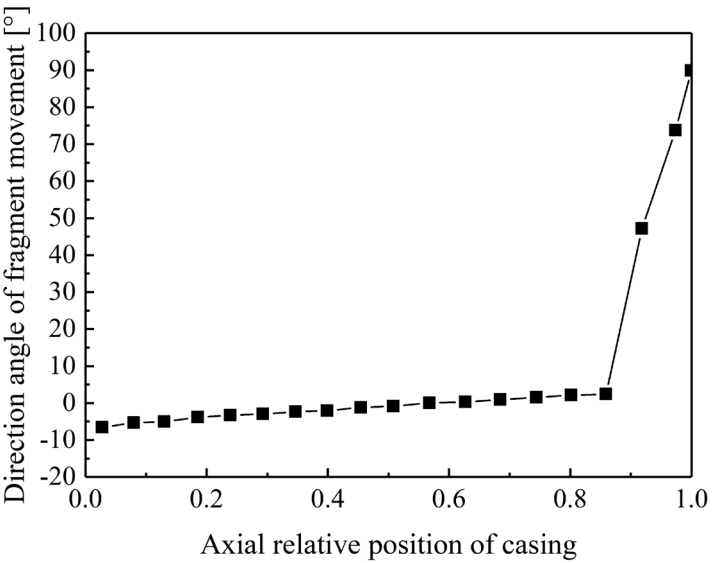

Figure 8. Theoretical results of fragment motion direction angle

Removing the geometric influence of the bottom of the warhead, combining with the total number of fragments M_{0i} and Equations 33 and 34 to form the fragment motion direction angle and its variance:

$$\varphi_0 = \frac{\sum_{i=1}^{15} \varphi_i M_{0i}}{147.52} = 3.4324° \tag{40}$$

$$\sigma_0 = \sqrt{\frac{\sum_{i=1}^{15} (\varphi_i - 3.4324)^2 M_{0i}}{147.52}} = 9.9512° \tag{41}$$

The methods described in the two references [11, 23] were used to calculate the average mass $\bar{m}_M$, volume fractal dimension D_3 and distribution modulus $\frac{2D_3 - 4}{3 - D_3}$ of the fragments formed at different coaxial parts of the warhead, and their variation rules were plotted as shown in Figure 9. In order to simplify the calculation, the average mass and volume fractal dimension of the fragment in the whole sense is used to study. According to the data in Figure 9, the average characteristic mass of the fragments formed by the warhead as a whole is $\bar{m}_M = 0.5321g$, the volume fractal dimension is $D_3 = 2.4257$, and the distribution modulus is $\frac{2D_3 - 4}{3 - D_3} = 1.4921$. By combining fragmentation spatial scattering results θ_0, σ_0 and Equation 26, the fragmentation mass/quantity density spatial distribution rule of the warhead at 1m away from the center of mass can be obtained, as shown in Figure 10.

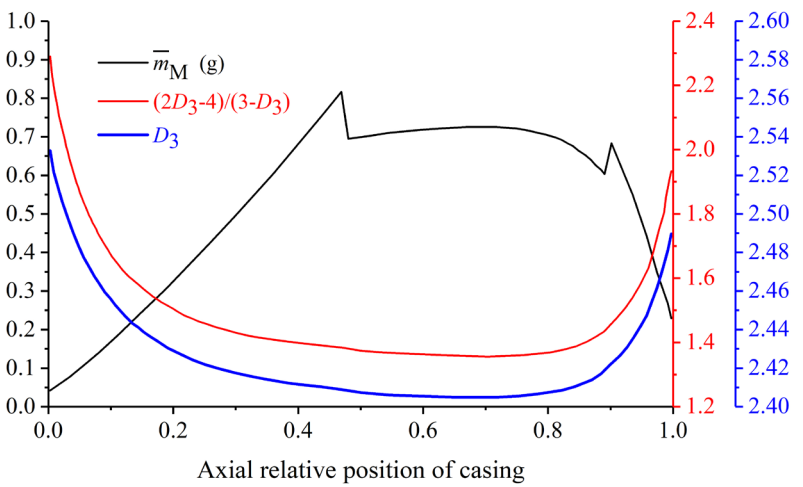

Figure 9. Related parameters of fragment mass distribution formed at different coaxial parts of warhead

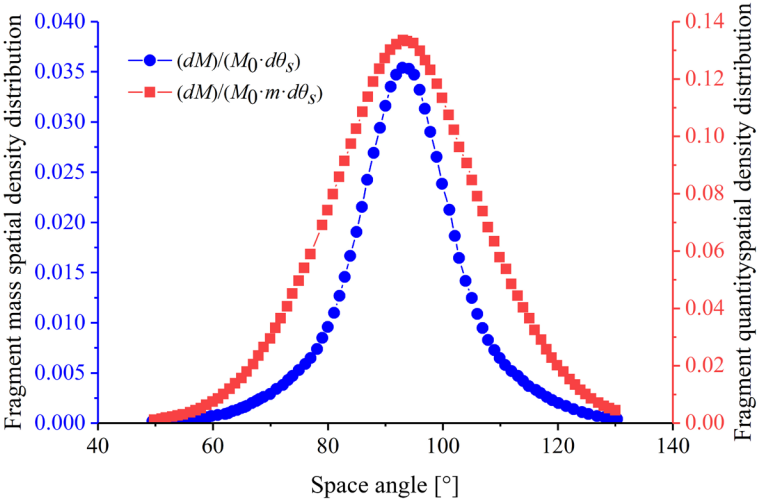

Figure 10. Spatial distribution law of fragment mass/quantity density

4.3 Comparison and analysis of theoretical calculation results and test results

The average number of fragments recovered was 892. According to θ_0 = 93.4324° and σ_0 = 9.9512° calculated above and combined with $N(\theta_i \sim \theta_{i+1}) = N_0 \int_{\theta_i}^{\theta_{i+1}} \frac{1}{\sqrt{2\pi}\sigma} e^{-\frac{(\theta_S-\theta_0)^2}{2\sigma^2}}$, the spatial distribution result of Mott fragment number can be calculated. Because the previous theory assumes that the fragment mass formed by the warhead is the same in space, the corresponding fragment mass spatial distribution results can also be directly calculated. The theoretical calculation results of this paper are compared with those of predecessors and test results, as shown in Figure 11. When the space angle θ_S is between 90° and 100°, the error between the theoretical calculation of fragment mass distribution and the test results is 4.3%, and the error between the theoretical calculation of fragment quantity distribution and the test results is 19.4%. This indicates that fragment mass is more suitable to characterize the spatial distribution of fragments than fragment quantity. This is because the quantity of fragments formed by the warhead is too random, and the mass of fragments is certain. When the space angle θ_S is in the range of 80°~100°, the prediction accuracy of the spatial distribution model of fragment mass proposed in this paper is 18.2% higher than that of the other model. This is because when analyzing the spatial distribution of fragments in the past, the mass of

fragments was considered to be consistent, which was obviously inconsistent with the actual situation. Therefore, in the past, both the theoretical calculation results of the spatial distribution model of fragment quantity and the theoretical calculation results of the spatial distribution of fragment mass derived from the spatial distribution of fragment quantity have great errors compared with the test results. In this paper, the uneven mass distribution of the fragments in different spatial angles interval is considered, so the theoretical results in this paper are closer to the test results.

The theoretical model in this paper can well describe the spatial distribution of fragment mass in the space angle of 80°~100°, but there are large errors between the theoretical and test results in other space angle ranges. However, as 84% of the total mass of the fragment is concentrated in the space angle range of 80°~100°, we can consider the theoretical model in this paper is reasonable.

On the whole, through the comparison and analysis of the theoretical results of this paper, previous theoretical results and test results, the rationality of the idea of using fragment mass to describe the spatial distribution of fragments proposed in this paper and the effectiveness of the fractal theory based natural fragment mass spatial distribution model established in this paper are illustrated. However, there are still some defects in the theoretical model. As the volume fractal dimension D_3 needs to be determined by the test results, the theoretical model in this paper cannot play a predictive role at present. To solve this problem, the author's team will conduct further research on volume fractal dimension D_3 in the future.

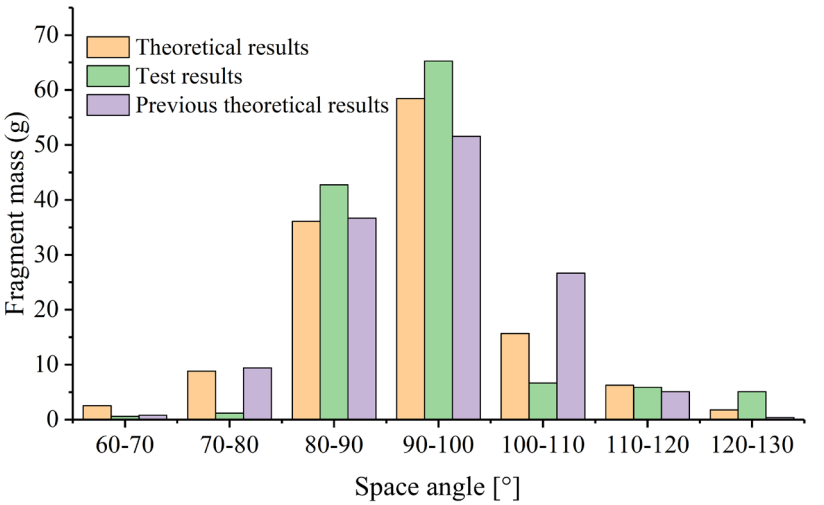

(a)

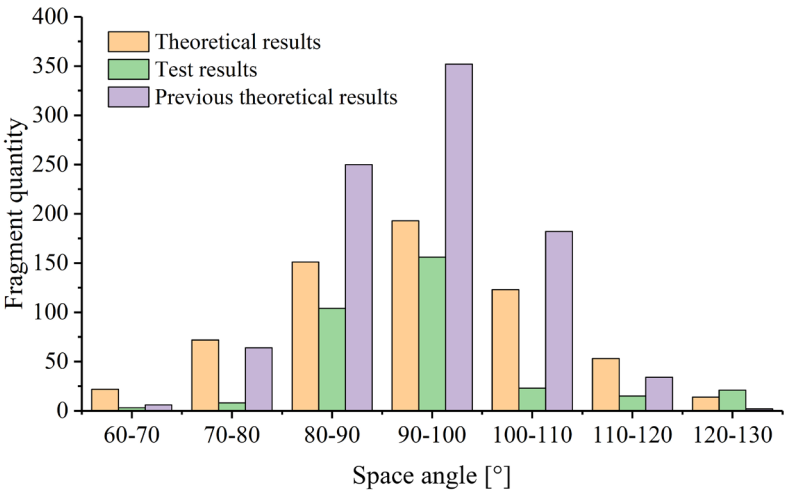

(b)

Figure 11. Comparison of the theoretical and experimental results of the spatial distribution of fragment mass (a) and quantity (b)

5 Conclusions

This paper mainly studies the relevant laws of natural fragmentation field formed by the killing warhead, including the spatial scattering characteristics of fragmentation and the spatial distribution law of fragmentation quantity/mass, and draws the following conclusions:

- Based on the thought of stress gradient grade and velocity gradient grade in the process of explosion, the calculation formula of the fragment direction Angle formed at different axial positions of warhead was established based on the modified Gurney formula, which solved the problem that the Shapiro formula could not describe the fragment scattering at the end of warhead. The model established in this paper can more accurately describe the variation law of fragment scattering in fragment space with the center of mass of warhead as the origin.
- Based on the fractal model of fragment mass distribution in the form of Weibull function, a two-dimensional joint probability density model of fragment space Angle and fragment mass was proposed, and the function form of fragment mass density exponential distribution was determined.
- Based on the principle of spherical target test, fragment recovery test

is carried out, and the test results are compared and analyzed with the theoretical results of this paper and the previous theoretical results. The results show that when the space angle θ_S is between 90° and 100°, the error between the theoretical calculation and the experimental results of the fragment mass distribution is 4.3%, which is 15.1% higher than the accuracy of describing the spatial distribution of the fragment by the fragment quantity. It indicates that the spatial distribution of fragment mass is more suitable to characterize the spatial distribution of fragment than the spatial distribution of fragment quantity. The accuracy of the spatial distribution model of fragment mass proposed in this paper is 18.2% higher than that of previous theoretical models, can more accurately describe the spatial distribution of fragments.

References

[1] Gurney, R.W. *The Initial Velocities of Fragments from Bombs, Shell and Grenades.* Ballistic Research Laboratories. Aberdeen Proving Ground, Report 405, US-MD, **1943**.

[2] Lloyd, R. *Conventional Warhead Systems Physics and Engineering Design.* American Institute of Aeronautics and Astronautics Inc., **1998**.

[3] Hutchinson, M.D. With-Fracture Gurney Model to Estimate both Fragment and Blast Impulses. *Cent. Eur. J. Energ. Mater.* **2010**, *7*(2):175-186.

[4] Mott, N.F. *A Theory of the Fragmentation of Shells and Bombs. Fragmentation of Rings and Shells.* Springer, Berlin/Heidelberg, **2006**, pp. 243-294.

[5] Kipp, M.E.; Grady, D.E. Dynamic Fracture Growth and Interaction in One Dimension. *J. Mech. Phys. Solids* **1985**, *33*(4): 399-415; https://doi.org/10.1016/0022-5096(85)90036-5.

[6] Mott, N.F. A Theory of the Fragmentation of Shells and Bombs. In: *Fragmentation of Rings and Shells: The Legacy of N.F. Mott*. (Grady, D.E., Ed.) Springer, Heidelberg, Berlin, Germany, **2006**, pp. 243-294.

[7] Held, M. Fragment Mass Distribution of HE Projectiles. *Propellants Explos. Pyrotech.* **1990**, *15*(6): 254-260; https://doi.org/10.1002/prep.19900150606.

[8] Zhu, J.J.; Li, W.B.; Wang, X.M.; Li, W.B. Effect of Tempering Temperature on Expansion and Fracture Mechanism of 40CrMnSiB Steel Cylinder Shell. *Int. J. Impact Eng.* **2017**, *107*: 38-46; https://doi.org/10.1016/j.ijimpeng.2017.05.007.

[9] Li, J.B.; Li, W.B.; Wang, X.M.; Li, W.B.; Hong, X.W. Mechanical Properties and Constitutive Model of Aluminum Powder/Rubber Matrix Composites Compressed at Various Strain Rates. *Int. J. Impact Eng.* **2018**, *121*: 55-62; https://doi.org/10.1016/j.ijimpeng.2018.07.005.

[10] Ma, T.; Yang, N.; Luo, Y.; Wang, Y.; Guo, G.; Wu, S.; Xu, S.; Wu, X. Effect of Aging

on Damage Properties and Reaction Characteristics of Typical 2,4-Dinitroanisole (DNAN)-based Melt-cast Explosives under Low-velocity Impact. *Propellants Explos. Pyrotech.* **2023**, *48*(12): paper e202300094; https://doi.org/10.1002/prep.202300094.

[11] Zhu, J.J.; Yu, Z.; Yang, Y.; Li,; W.; Wang, X.; Li, W.; Qiao, X. Research on the Volume and Line Fractal Dimension of Fragments from the Dynamic Explosion Fragmentation of Metal Shells. *Powder Technol.* **2018**, *331*: 129-136; https://doi.org/10.1016/j.powtec.2018.01.084.

[12] Yang, Y.C. Study on Fractal Mathematical Models of Pulverizing Theory for Ore. *Powder Technol.* **2016**, *288*: 354-359; https://doi.org/10.1016/j.powtec.2015.10.050.

[13] Dhote, K.D. Statistics of Fragment Dispersion by Explosion in a Fragment Generator Warhead. *Cent. Eur. J. Energ. Mater.* **2016**, *13*(1): 183-197.

[14] Li, L.P. *Investigation on some Key Measuring Technologies of Fragment Warhead Power Field.* Doctoral dissertation, Nanjing University of Science and Technology, Nanjing, **2017**.

[15] Huang, J.W. *Study on Fragment Law of Fragment Warhead and Fragment Penetration Effect on Infantry Fighting Vehicle.* Doctoral dissertation. Nanjing University of Science and Technology, Nanjing, **2014**.

[16] Grisaro, H.Y.; Dancygier, A.N. Spatial Mass Distribution of Fragments Striking a Protective Structure. *Int. J. Impact Eng.* **2018**, *112*:1-14; https://doi.org/10.1016/j.ijimpeng.2017.10.003.

[17] Karpp, R.R.; Predebon, W.W. Calculations of Fragment Velocities from Naturally Fragmenting Munitions. *Proc. 1st Int. Symp. Ballistics*, **1974**, pp. 145-176.

[18] Wang, S.S. *Terminal Effects*. Science Press, Beijing, **2019**.

[19] Huang, G.Y.; Li, W.; Feng, S.S. Axial distribution of Fragment Velocities from Cylindrical Casing under Explosive Loading. *Int. J. Impact Eng.* **2015**, *76*: 20-27; https://doi.org/10.1016/j.ijimpeng.2014.08.007.

[20] Zhu, J.J.; Li, W.B.; Wang, X.M.; Cheng, X.W.; Li, W.B.; Lu, H.T. Effect of Tempering Temperature on the Forming Properties of Fragments of 50SiMnVB Steel Shell. *Acta Armamentarii* **2015**, *36*(11): 2080-2086; https://doi.org/10.3969/j.issn.1000-1093.2015.11.009.

[21] Li, J.B.; Li, W.B.; Yu, J.X.; Xiao, W.; Xu, H.Y. Blast Performance of Layered Charges Enveloped by Aluminum Powder/Rubber Composites in Confined Spaces. *Def. Technol.* **2022**, *18*(4): 583-592; https://doi.org/10.1016/j.dt.2021.03.014.

[22] Alphin, H.E. *Research and Development of Material. Engineering Design Handbook.* Headquarters, United States Army Material Command, Washington, US-DC, **1962**.

[23] Zhu, J.J.; Zheng, Y.; Li, W.; Yang, Y.; Wang, X.; Qiao, X.; Li, R. Axial Distribution of Fragments from the Dynamic Explosion Fragmentation of Metal Shells. *Int. J. Impact Eng.* **2018**, *123*: 140-146; https://doi.org/10.1016/j.ijimpeng.2018.09.020.

[24] Xin, C.L. *Handbook of Common Material Parameters for Finite Element Analysis.* China Machine Press, Beijing, **2019**.

[25] Li, J.B.; Li, W.B.; Hong, X.W.; Yu, J.X.; Zhu, J.J. Blast Wave Characteristics of

Multi-layer Composite Charge: Theoretical Analysis, Numerical Simulation, and Experimental Validation. *Def. Technol.* **2021**, *19*: 91-102; https://doi.org/10.1016/j.dt.2021.11.012.

[26] Mirzaei, M.; Tavakoli, S.; Najafi, M. On the Role of Stress Waves in Dynamic Rupture of Cylindrical Tubes. *Fatigue Fract. Eng. Mater. Struct.* **2017**, *40*(12): 2008-2018; https://doi.org/10.1111/ffe.12621.

Received: February 15, 2023
Revised: March 28, 2024
First published online: June 28, 2024